Izv. VUZ «AND», vol.10, № 3, 2002

OPTICAL PROPERTIES OF COLLOIDAL-GOLD BIOCONJUGATES

N. G.Khlebtsov, V.A. Bogatyrev, L.A. Dykman,
Ya.M. Krasnov, A.G. Melnikov

We discuss optical properties of single or aggregated colloidal-gold conjugates that can be fabricated by adsorption of a biopolymer onto the surface of nanoparticles. To simulate extinction and scattering of light by such structures, we apply the generalized multisphere Mie solution and the discrete dipole approximation along with a computer model of cluster-cluster aggregation. Our consideration includes the following topics: statistical and orientational averaging of optical observables; optical effects related to the chain-like structures; effects of polymer coating and interparticle spacing; simulation of kinetic changes in the optical properties of aggregated sols formed during biospecific binding; modification of the exact multipole approach for the case of two-layered monomers. In the rest of this paper, we give a short review of our experimental work on the topic (including biomedical applications) and provide experimental examples concerning the optical monitoring of biospecific interactions on a nanometer scale.

1. Introduction

Colloidal-gold (CG) nanoparticles have been widely used during the past years as effective optical transducers of biospecific interactions [1]. In particular, the resonance optical properties of nanometer-sized CG particles have been employed to design biochips and biosensors [1-3] used as analytical tools in biology (determination of DNA, RNA, proteins, and metabolites), medicine (drugs screening, antigen and antibody determination, virus and bacterial diagnostics), and chemistry (on-line environmental monitoring, quantitative analysis of solutions and disperse media). As a special and important example one should note polynucleotide detection, based on the formation of 3-D ordered structures that result from hybridizing conjugate linkers with complementary oligonucleotides [4, 5]. These systems can potentially detect femtomolar concentrations of oligonucleotides [1].

It is well known [6, 7] that the surface plasmon resonance (SPR) of gold nanoparticles near 520 nm controls the characteristic spectral properties of colloidal-gold sols. The formation of aggregated structures results in substantial changes in the value and spectral position of SPR because of the strong electrodynamic interaction of cluster gold particles when their average spacing is comparable to or less than the particle size [8, 9]. This strategy (analogous to the sol-particle immunoassay, SPIA [10]) can be applied to protein detection at nanogram level [11] as well as to sensitive clinical diagnostics [12, 13]. It is clear that optimization of the nano-gold-markers methodology

demands a deep insight into the optical properties of conjugates and aggregates built from these monomers. However, noticeable progress in the field has been achieved only very recently because of the strong electrodynamic many-particle interaction of cluster nanoparticles when its spacing is less than their size [14].

This paper gives an overview of our recent work (including the work supported by CRDF grant REC-006) [14-23] related to theoretical and experimental studies of extinction and light scattering properties of colloidal gold bioconjugates and to some biomedical applications of the markers developed [24-29]. Besides we present here some new data that have not been published anywhere before.

2. Theoretical study

2.1. Computer model for cluster aggregation. A three-dimensional lattice model with Brownian or linear trajectories of single particles and intermediate clusters was employed to simulate the aggregation process. At the initial time moment, N_0 particles are generated at randomly selected points of a cubic lattice with size L. When a particle moves to a lattice point adjacent to another particle or intermediate cluster, a combined cluster is formed. This model produces diffusion-limited (Brownian trajectories) or ballistic (linear trajectories) clusters with fractal dimension $d_f \approx 1.8$ and $d_f \approx 2.0$, respectively. A more detailed description of the model can be found elsewhere [30].

2.2. Light scattering and extinction by a single aggregate.

2.2.1. Discrete dipole approximation (DDA). Consider the scattering of a plane electromagnetic wave propagating in a dielectric surrounding medium with the refractive index n_0

$$\mathbf{E}_0 = \mathbf{e}_0 \exp(\hat{\imath}\mathbf{kr}), \quad |\mathbf{e}_0| = 1, \quad |\mathbf{k}| = k = 2\pi n_0/\lambda, \quad \hat{\imath} = (-1)^{1/2}, \tag{1}$$

by a single cluster built from N small spherical nanoparticles with radius a and complex refractive index $n(\lambda)$. In the DDA method [31], a real aggregate is replaced by a set of point dipoles $\mathbf{d}_i = \mathbf{d}(\mathbf{r}_i)$, i=1-N. The linear equations for the interacting dipoles can be written in the form [16]

$$\Sigma_{jm=1}^{3N} A_{il,jm} d_{jm} = \alpha_i e_{0l} \exp(\hat{\imath}\mathbf{kr}_i), \quad il = 1 - 3N, \tag{2}$$

where α_i is the polarizability of the ith dipole, the combined indices are il=3(i-1)+l, jm=3(j-1)+m; i,j=1-N; and indices l,m=1,2,3 (x,y,z) correspond to the Cartesian components of vectors or tensors. The explicit form of the dipole interaction matrix $A_{il,jm}$ can be found in Ref. [16]. The solution of the linear systems of Eqs. (2) allows one to calculate all the basic optical characteristics of the aggregate. For instance, the extinction cross section, determining the spectrum of optical density of a dilute suspension, can be calculated from the optical theorem [6, 14]

$$C_e = 4\pi k \mathrm{Im}\Sigma_i \, (\mathbf{e}_0 \mathbf{d}_i) \exp(-\hat{\imath}\mathbf{kr}_i). \tag{3}$$

In the above sketch description we omitted some important questions related to the choice of optical polarizability and renormalization of interdipole spacing. The readers are referred to the corresponding discussion in review [14] and to the references therein. In short, we used the interparticle spacing parameter $\gamma = d_L/a$ as a fitting parameter of a theory providing for the best agreement between theoretical predictions and experimental observations [32].

In practical applications, one usually needs average results for random orientations

of clusters rather than calculations for a particular structure with a fixed orientation. In principle, such averaging can be carried out by numerical integration over Euler angles that define the orientation of a scatterer with respect to the incident wave. However, an analytical solution of such a problem turns to be much more effective as compared with the straightforward numerical approach. Examples of such analytical solutions are well known in the T-matrix method including its application to the cluster light scattering [14]. In works [18, 20], we derived an exact analytical solution for integral extinction, scattering, and absorption DDA cross sections averaged over random orientations of scatterers. Application of the solutions was illustrated by practical computations of averaged extinction cross sections for several examples of fractal clusters (soot in air and colloidal aggregates built from polystyrene, gold, or silver nanoparticles).

The interaction matrix in Eq. (2) does not depend on the incident wave orientation, so it is convenient to perform orientational averaging in the cluster coordinate frame. Using the inverse matrix $B=A^{-1}$ to solve Eq. (2), we obtain the following general equation for the extinction cross section

$$\langle C_e \rangle = 4\pi k \mathrm{Im}\{\Sigma_{i,j=1}^{N} \Sigma_{p,q=1}^{3} \alpha B_{ip,jq} E_{pq}^{ij}\}, \quad E_{pq}^{ij} = \langle \tilde{V}_{pq} \exp(-\hat{\imath}\mathbf{k}\mathbf{r}_{ij}) \rangle, \tag{4}$$

where the angle brackets mean integration over Euler angles that define the orientation of the incident wave in the cluster frame, $\tilde{V}_{pq} = e_p e_q$ is the second-rank tensor, and e_p are the Cartesian components of the polarization vector in the cluster frame. The general scheme for calculation of average cross sections according to Eq. (4) consists in the following: First, we represent the tensor $\tilde{V}_{pq}$ as a linear combination of irreducible spherical tensors in the incident wave coordinate frame. Such a transformation can be performed using Clebsh-Gordan coefficients and Wigner rotation functions [14]. Then, we expand the plane incident wave in a series over vector spherical harmonics (VSH) and perform orientational averaging by using the orthogonality properties of VSH and Wigner functions. Omitting the technical details of calculations, we give the final result:

$$\langle C_e \rangle = 4\pi k \mathrm{Im}\{\mathrm{Spur}(T)\}, \quad \langle C_a \rangle = 4\pi k \mathrm{Spur}(W), \tag{5}$$

where the matrices T and W are defined by equations

$$\hat{A}\hat{T} = \alpha\hat{E}, \quad W = \eta|\alpha|^2 \hat{B}\hat{E}\hat{B}^{+}, \tag{6}$$

and the explicit form of parameter η and an auxiliary matrix E can be found in Refs. [18,20].

2.2.2. Generalized multiparticle Mie solution (GMM). For large dielectric monomers or metal nanoparticles, the DDA model fails because of the multipole nature of electrodynamic particle coupling. An exact solution of the cluster-light-scattering problem can be formulated rather simply, using a generalized Mie theory for multisphere configurations [33, 34]. An incident electromagnetic field $\mathbf{E}_{inc}{}^{i}$ for the ith particle can be expanded over VSH $\mathbf{Y}_{mn1}^{(\tau)} = N_{mn}^{(\tau)}(k\mathbf{r}_i)$; $\mathbf{Y}_{mn2}^{(\tau)} = \mathbf{M}_{mn}^{(\tau)}(k\mathbf{r}_i)$ of the first kind (τ=1; spherical Bessel generating functions are used)

$$\mathbf{E}_{inc}{}^{i} = \Sigma_{n=1}^{\infty} \Sigma_{m=-n}^{n} \Sigma_{p=1}^{2} \hat{\imath} E_{mn} p_{mnp}{}^{i} \mathbf{Y}_{mnp}^{(1)}(k\mathbf{r}_i), \tag{7}$$

where E_{mn} are normalization coefficients. For a plane wave (see Eq. (1)) with the incidence direction defined by Euler angles ($\varphi=\alpha$, $\vartheta=\beta$, $\psi=\gamma$) in the ith coordinate frame, the expansion coefficients are

$$\bar{p}_{mnp}{}^{i} = \exp(\hat{\imath}\,\mathbf{k}\mathbf{r}_i) \exp(-\hat{\imath}m\varphi) 1/n(n+1)[\tau_{mnp}(\vartheta)\cos\psi - \hat{\imath}\tau_{mn3-p}(\vartheta)\sin\psi], \tag{8}$$

$$\mathbf{kr}_i = k[x_i \sin\vartheta \cos\varphi + y_i \sin\vartheta \sin\varphi + z_i \cos\vartheta], \quad (9)$$

where the functions $\tau_{mnp}(\vartheta)$ (p=1, 2) correspond to the well-known light scattering functions $\tau_{mn}(\cos\vartheta)$, $\pi_{mn}(\cos\vartheta)$ [6].

The scattered field from the i-th particle can be expanded over VSH of the third kind (Hankel generating functions are used) in the same manner as in Eq.(6)

$$\mathbf{E}_s^i = \Sigma_{n=1}^{\infty} \Sigma_{m=-n}^{n} \Sigma_{p=1}^{2} iE_{mn} a_{mnp}^i \mathbf{Y}_{mnp}^{(3)}(k\mathbf{r}_i). \quad (10)$$

The application of the usual boundary conditions leads to the following simple relations between the expansion coefficients

$$a_{mnp}^i = \bar{a}_{np}^i p_{mnp}^i, \quad (11)$$

where $\bar{a}_{n1}^i = \bar{a}_n^i$, $\bar{a}_{n2}^i = b_n^i$ are the usual Mie coefficients for an isolated homogeneous sphere [6]. Solution (11) is a crucial one in the GMM as it gives a simple and exact relation between p_{mnp}^i (exciting field) and a_{mnp}^i (scattered field). The unknown expansion coefficients of the exciting field can be found from the superposition principle that leads to the set of linear equations

$$\Sigma_{j=1}^{N} \Sigma_{\nu=1}^{\infty} \Sigma_{\mu=-\nu}^{\nu} \Sigma_{q=1}^{2} H_{mnp,\mu\nu q}^{ij} p_{\mu\nu q}^j = \bar{p}_{mnp}^i, \quad (12)$$

where $\bar{p}_{mnp}^i$ are the known expansion coefficients of the incident field in the ith coordinate frame. The interaction matrix H is determined by the «coefficients of translation» of VSH based on spherical Hankel functions of the first kind (see explicit relations in Ref. [14]).

Once Eqs (12) are solved and coefficients a_{mnp}^i are found, one can calculate all characteristics of light scattered by a cluster. For example, the extinction cross section is given by equation

$$C_e = 4\pi/k^2 \Sigma_{i=1}^{N} \Sigma_{n=1}^{M} \Sigma_{m=-n}^{n} \Sigma_{p=1}^{2} C_{mn} \mathrm{Re}[a_{mnp}^i (\underline{p}_{mnp}^i)^*], \quad (13)$$

where coefficients C_{mn} depend on VSH normalization. The light scattering observables can be averaged over random cluster orientations by using T-matrix cluster formulation and the corresponding theorems for orientational averaging [34, 35].

2.3. Calculation of extinction and light scattering spectra for ensembles of clusters. A model for the dynamic simulation of extinction spectra during the aggregation process was developed in our work [16]. We assume that a cluster suspension is dilute so that the single scattering approximation is valid. This means that the extinction (optical density or absorption) $A(\lambda)$ is directly proportional to the sum of extinction cross sections of clusters per unit volume. It is convenient to normalize the extinction spectra to the monomer optical density $A_m(a, \lambda_{max})$ at the maximum of extinction of monomers $C_{em}(\lambda_{max})$

$$A_m(\lambda) \equiv A(a, \lambda)/A_m(a, \lambda_{max}) = C_e(a, \lambda)/C_{em}(a, \lambda_{max}). \quad (14)$$

The cluster-size distribution at an arbitrary stage of aggregation can be described by a set of number pairs (p, N_p), where p is the number of particles per aggregate from a given monodisperse ensemble (p, N_p), and N_p is the number of such aggregates. Light extinction by the (p, N_p) ensemble is given by the normalized extinction cross section

$$\langle \overline{Q_p} \rangle = \langle \overline{C_{ep}(R_m, \lambda)} \rangle / pC_{em}(R_m, \lambda), \quad (15)$$

where the angle brackets denote the averaging over random cluster orientations in a monodisperse ensemble of clusters, and the horizontal bar designates statistical averaging

over cluster configurations of ensemble (p,N_p). The optical density of the suspension is given by the relationship

$$E(\lambda) = E_m(R_m,\lambda)\Sigma_p \nu_p \langle Q_p \rangle, \tag{16}$$

where ν_p is the fraction of p-cluster particles of the total number of initial monomers N_0

$$\nu_p = pN_p/\Sigma_p pN_p = pN_p/N_0. \tag{17}$$

For calculation of the absolute values of extinction and scattering intensity, we used a gold concentration of gold 57 μg/ml (cuvette thickness 1 cm).

2.4. Statistical and orientational averaging of light scattering observables: some important simplifications. It is clear that calculation of $\overline{\langle C_{ep} \rangle}$ quantities is a challenging step of the simulations. In both methods (DDA and GMM), the analytical procedures of orientational averaging imply that the cluster T-matrix (i.e., actually, the corresponding inverse interaction matrix) has to be found. At moderate numbers of cluster particles (say, $N \leq 3000$), the DDA analytical method can be implemented in a usual PC without any problem. However, the GMM analytical solution needs a huge RAM volume even for small ($N \sim 100$) metal clusters because of the multipole nature of the electrodynamic interaction (see discussion in Refs. [14, 34]). Having in mind that actually we need both orientational and statistical averaging over cluster configurations, we encounter a serious calculation problem.

However, these difficulties suggest that statistical averaging over a *large number of random configurations* is perhaps all we need. In other words, we can hazard a conjecture that statistical averaging actually includes the orientational one. Symbolically, our hypothesis can be written as follows:

$$\overline{\langle C_{ep} \rangle} \approx \overline{C_{ep}}. \tag{18}$$

To verify this hypothesis, we generated monodisperse statistical ensembles of clusters with N=const. and then calculated two sets of the averaged parameters, for example $\overline{\langle C_e \rangle}$ and $\overline{C_e}$. Two quantities were computed: the extinction cross section C_e, or the corresponding absorption A_e, and the normalized scattered intensity $S_{90}=S(\theta=90)$[1] (for simplicity, we will subsequently omit the subscript 90). Some data obtained are listed in Table. We drew two important conclusions from these results: First, to simulate the extinction of light by an aggregated suspension, it is sufficient to account only for random cluster configurations, i.e., without orientational randomization. Second, the scattered intensity is more sensitive to cluster orientations than extinction is. Therefore, one has to use a big statistical monodisperse ensemble in order to eliminate fluctuations in the calculated scattered intensity. The first conclusion leads to great simplifications, as we can use effective and fast codes for clusters with fixed orientations instead of huge RAM consuming codes for analytical T-matrix averaging.

2.5. Effects of aggregate form and interparticle spacing. Looking at the internal structure of real or simulated clusters, one can note numerous chain-like fragments. Therefore, it would be desirable to understand possible optical effects related to the formation of such chain-like nanoparticle structures. We can make a rough-cast evaluation by using a homogeneous spheroidal model that can be easily treated by the T-matrix method [14]. Fig. 1 shows the spectral dependence of extinction calculated for randomly oriented spheroids with equivolume radius 30 nm and axis ratio $e=a/b$=1, 1.3,

[1] Along with our own routines, we used numerical codes gmm01s and scsmtm1, kindly provided by Yu-lin Xu (Univ. of Florida, USA) and Daniel Mackowski (Auburn Univ., USA). Thanks to both colleagues.

Table

Comparison of extinction $A_1 \equiv \overline{A_{ext}}$, scattered intensity $S_1 \equiv \overline{S_{90}}$ (statistical averaging only) and $A_2 \equiv \langle \overline{A_{ext}} \rangle$, $S_2 \equiv \langle \overline{S_{90}} \rangle$ (both orientational and statistical averaging). Calculations for clusters built from N=10 or 100 gold particles with diameters 15 and 30 nm coated by 2.5 nm polymer shell with n_2=1.4. All data are averaged over 100 independent cluster configurations.

d, nm	N	λ=400 nm				λ=500 nm				λ=600 nm			
		A_1	A_{2c}	S_1	S_{2c}	A_1	A_{2c}	S_1	S_{2c}	A_1	A_{2c}	S_1	S_{2c}
15nm	10	.665	.664	.189	.185	.955	.954	.176	.174	.213	.213	.163	.161
	100	.674	.672	.275	.278	.922	.921	.364	.368	.296	.298	.589	.603
30nm	10	.711	.708	.763	.744	.894	.893	.779	.766	.551	.545	.201	.195
	100	.671	.667	.448	.470	.777	.775	.487	.513	.904	.897	.256	.251

1.5, and 2. The optical constants of gold and the surrounding medium (water) were calculated according to Ref. [36]. With an increase in the axis ratio, one can observe the red shift of the extinction maximum and the appearance of a short wavelength mode (peak splitting [6]). Fig. 2 shows extinction spectra calculated for a randomly oriented linear chain of 13-nm gold spheres with interparticle spacing 1.1 nm. Again, one can observe a noticeable red shift of peaks and its splitting. Note that our results essentially differ from the data published recently by Lazarides and Schatz [37]. Perhaps, their Fig. 8 from [37] was calculated with an insufficiently large multipole expansion order.

The interparticle distance Δd is a key parameter that determines the electrodynamic coupling of gold monomers. We have shown [16] that for clusters built from contacting silver or gold nanospheres, the convergence of the GMM method is too slow due to the multipole nature of the interparticle interaction. However, if the cluster particles are separated by a small distance, the number of multipole terms in a series is decreased down to a tractable level. This effect is illustrated in Fig. 3, where the

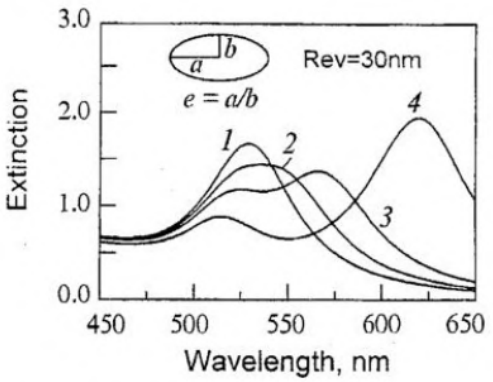

Fig. 1. Extinction spectra of randomly oriented gold nanospheroids in water. The equivolume diameter d_v=30 nm and axis ratio e=a/b=1(sphere *1*), 1.3 (*2*), 1.5 (*3*), and 2 (*4*)

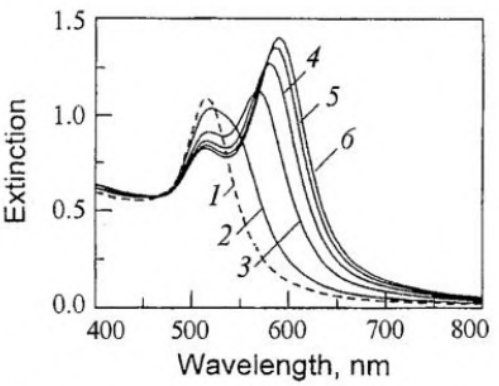

Fig. 2. Extinction spectra of randomly oriented chains built from 13 nm gold particles separated by 1 nm distance in water. The number of spheres equals to 1 (*1*), 2 (*2*), 4 (*3*), 6 (*4*), 8 (*5*), and 10 (*6*)

normalized extinction cross section $Q_{ev}=C_e/\pi a_v^2$ (a_v is the equivolume cluster radius) is plotted as a function of multipole order at different distances between particles. The parameters of the model (a=6.2 nm, λ=520 nm) correspond to the surface plasmon resonance of monomers. Generally, our data concerning this point are in agreement with the data of Ref. [38].

2.6. Optical properties of two-layered gold conjugates. Adsorption of a biopolymer onto gold nanoparticles results in the formation of a complex structure that can be approximated by a simplest two-layered model: gold core + homogeneous polymer shell, as it was introduced in our work [36]. Recently, the importance of this model was emphasized in relation to the optimization of a colorimetric gold nanoparticle sensor [39] and to the studies of adsorption phenomena [40]. We have studied the optical properties of a two-layered model for gold bioconjugates in detail. Here, we present only illustrative examples of the simulations.

In our calculations, the polymer shell was treated as homogeneous nonabsorbing dielectric with refractive index n_2=1.4 or 1.5. The shell thickness s was equal to 5 or 10 nm and was close to the sizes of globular proteins. The refractive index of bulk gold $n_1=n_1(\lambda)$ was used for the conjugate core. Fig. 4 shows changes in extinction spectra caused by polymer adsorption (s=5 nm, n_2=1.5 at c_g=const=57 μg/ml). Increasing the shell thickness and their refractive index leads to a corresponding increase in optical effects. The maximal extinction and scattering are observed for particle diameters 60 nm; however, the maximal *relative* change in extinction and scattering

$$\delta A = [A(\lambda_{ext}^{max}, s=5) - A(\lambda_{ext}^{max}, s=0)] / A(\lambda_{ext}^{max}, s=0), \quad (19)$$

$$\delta S = [S(\lambda_{sca}^{max}, s=5) - S(\lambda_{sca}^{max}, s=0)] / S(\lambda_{sca}^{max}, s=0), \quad (20)$$

is observed for the smallest (10-nm) particles (Fig. 5, dashed curves). The red shift of extinction and scattering is also maximal for the smallest particles and then decreases with an increase in the particle diameter (up to 80 nm). On the other hand, the finest particles have a higher polymer adsorption capacity. Therefore, to estimate the efficiency

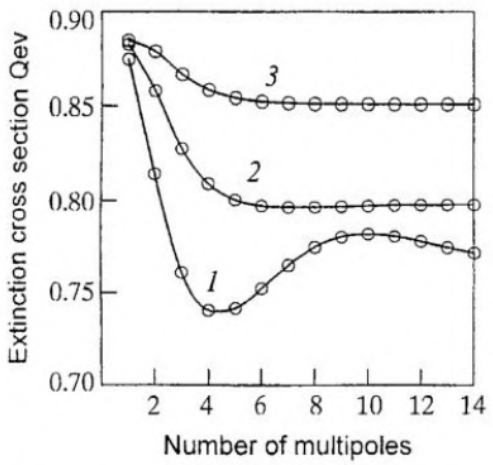

Fig. 3. Dependence of the normalized extinction cross section $Q_{ev}=C_e/\pi a_v^2$ on the number of multipoles included in VSH expansions of the GMM method. Calculations for randomly oriented bispheres (d=2a=12.4 nm, λ=520 nm) in contact Δd=0.0 (*1*) and separated by distances Δd=0.05d (*2*) and Δd=0.1d (*3*) in water

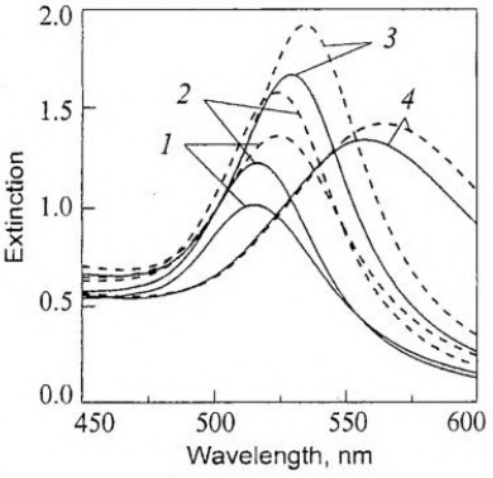

Fig. 4. Extinction spectra of gold particles in water (diameters d=10 (*1*), 20 (*2*), 60 (*3*), and 100 (*4*) nm, solid lines) and the same particles coated by a 5-nm polymer shell with the absolute refractive index n_2=1.5 (dashed lines)

of optical response per adsorbed polymer molecule, we introduce the SPIA efficiency parameter[2]

$$E = \text{(optical effect)/(polymer adsorption)} \sim \text{(optical effect)}\ /\delta V, \qquad (21)$$

where $\delta V=(a+s)^3/a^3-1$ is the relative change in the volume of a conjugate. For example, for the relative changes in light absorption and scattered intensity δS, we have

$$E_A=\delta A/\delta V,\quad E_S=\delta S/\delta V. \qquad (22)$$

The solid lines in Fig. 5 show the dependencies of the efficiency parameters E_A and E_S calculated for s=5 nm and 10 nm, n_2=1.4, c_g=const=57 μg/ml. It is clear that 60-nm gold particles are the best optical transducers of biospecific interactions that result in adsorption of biopolymers onto the particle surface. We also studied another situation when the polymer and gold concentrations were fixed whereas the particle diameter was considered as an optimization parameter. Again, we concluded that 60-nm particles gave the highest optical response. A more detailed consideration will be published separately.

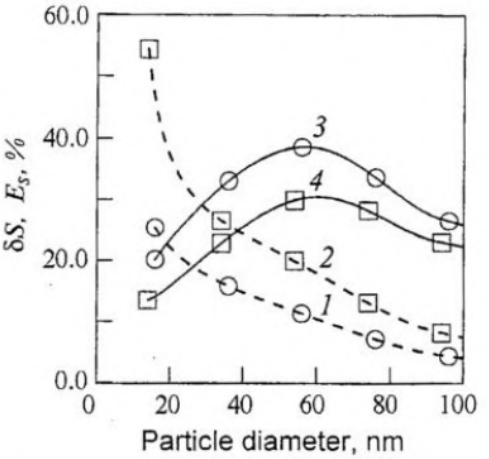

Fig. 5. Dependences of the relative change in scattering δS(dashed lines) and the SPIA efficiency parameter E_S (solid lines) on the diameter of gold particles (in water) coated by a 5-nm (curves 1 and 3) and a 10-nm (curves 2 and 4) polymer shell with the absolute refractive index n_2=1.4

2.7. Dynamic simulation of optical effects caused by particle aggregation. To simulate the temporal dynamics of extinction and scattering spectra during the aggregation process, we introduced the following model [15]: The time corresponding to the formation of 10 new clusters in a system was used as a sample time interval. After each interval, the cluster-size distribution function was determined and the corresponding spectra were calculated according to the procedure described in Section 2.3. The simulations were performed by the DDA method with intersection parameter $\gamma=(4\pi/3)^{1/3}$ = =1.612 on a lattice with size L=46 and the number of initial monomers N_0=500 (the monomer density $\rho=N_0/L^3\approx0.005$). Almost identical data were obtained during larger-scale simulations with L=58, N_0=1000. The dynamic simulation was terminated after the cluster with size N=200 had been generated. To smooth the statistical fluctuations, we repeated all calculations by using independent cluster generations and then averaged the theoretical spectra. Fig. 6 shows an example calculated for 15-nm monomers, the curves in the figure correspond to 100 newly formed aggregates. The appearance of the secondary absorption peak in the red region and the complex dynamics of the spectra resemble to a large extent, our experimental observations. For a deeper consideration, the readers are referred to Ref. [15].

2.8. Exact multipole model for clusters built from two-layered conjugates. To simulate the aggregation of colloidal-gold biomarkers, we introduce an exact multipole model based on a combination of the GMM method and the two-layered model for a single bioconjugate. The above consideration of GMM in Section 2.2.2 shows that all

---

[2] One of variants SPIA technique is based on measurements of small changes in extinction caused by adsorption of biopolymers onto surface of gold nanoparticles [12, 13].

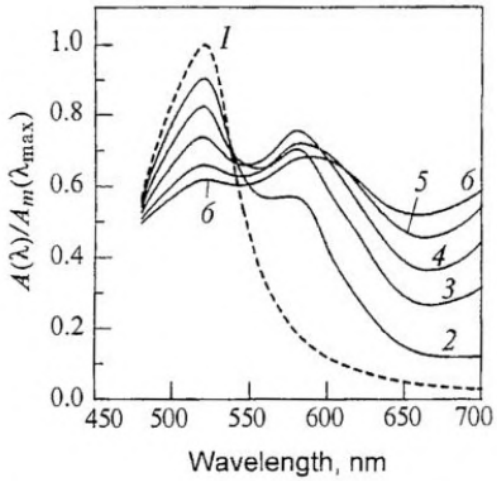

Fig. 6. Theoretical extinction spectra calculated for 15-nm gold sol at different stage of aggregation (dynamic simulation). Dashed curves correspond to single particles, curves 2-6 were calculated by using DLCA aggregation model and the modified DDA method with renormalization lattice parameter γ=1.62. The number near curves designate sequential time moments corresponding to the formation of 100 new clusters

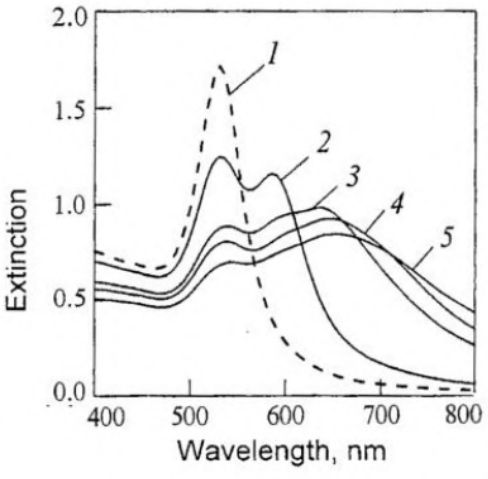

Fig. 7. Theoretical extinction spectra calculated by the exact GMM method for aggregates built from *1* (dashed line), 2 (*2*), 10 (*3*), 20 (*4*) and 50 (*5*) two-layered monomers (core-mantle model of a bioconjugate: 60 nm gold core and 2.5 nm polymer shell, n_2=1.4). All spectra were averaged over random orientations of clusters and over 10 statistical configurations of monomers

optical properties of an *i*th monomer are included in the single-particle coefficients $\bar{a}_{np}^{\,i}$. It is clear that the GGM solution can be applied to an arbitrary monomers that possess spherical symmetry. Therefore, one can generalize the standard GMM solution by replacing the well-known Mie coefficients for a homogeneous sphere with its two-layered analogs [6]. We have made the corresponding modifications of our GMM codes and the codes received from Yu-lin Xu and D. Mackowski. These modified codes were tested by benchmark computations performed independently in our laboratory and in the University of Florida, by Yu-lin Xu. At present, the exact two-layered multipole model is extensively used in simulation of the optical properties of aggregated conjugates. An illustrative example is shown in Fig.7. The extinction spectra were calculated for aggregates built from 1, 2, 10, 20, and 50 gold conjugates. The core diameter was 60 nm and the shell thickness was 2.5 nm, n_2=1.4, so that the interparticle distance was 5 nm. The spectra of individual clusters were averaged over random orientations and additionally averaged over 10 cluster configurations. As in Fig.6, the aggregation results in the appearance of additional red-shifted peak of extinction. This effect is observed at a rather small number of monomers, because the average cluster size is large enough due to the large diameter of monomers.

3. Experimental

3.1. Materials and methods. In this Section, we give a short review of our experimental results related to the optics of colloidal-gold conjugates. Colloidal-gold particles were synthesized according to procedures described in Refs. [16, 36], by reducing tetrachloroauric acid with sodium citrate. The protocol for preparing conjugates of CG to biospecific macromolecules, which involves preparing and purifying an aqueous probe solution, determining the «gold number», coupling the probe to the label, adding a

secondary stabilizer, concentrating the marker, and optimizing the end product, has been described elsewhere [41].

3.2. Optical properties of clusters formed during slow and fast aggregation. Our first experimental study [16] was related to the optical properties of colloidal gold aggregates formed during aggregation initiated by addition of the NaCl salt. The extinction spectra (400-800 nm) of aggregates of colloidal-gold particles (diameters 5, 15 and 30 nm) and silver particles (diameter 20 nm) were studied experimentally and theoretically. We have found that during fast aggregation corresponding to the formation of the diffusion-limited (DLCA) clusters, the spectra were dependent on the size of the primary particles. For aggregates of 15- and 30-nm gold particles and for 20-nm silver particles, we recorded spectra with an additional red extinction maximum, whereas the extinction spectra for aggregates of 5-nm particles had a single red-shifted extinction maximum. The slow aggregation resulted in a decrease in the plasmon extinction peak (without an essential red shift) and in the broadening of the long-wavelength extinction wing. According to the TEM data, the fast aggregation gave typical ramified DLCA aggregates, whereas the slow aggregation led to small compact structures along with an appreciable number of single (not aggregated) particles. To explain these findings, we used a computer diffusion-limited cluster-cluster aggregation model. The optical properties of the aggregates were computed by the coupled dipole method (CDM or DDA) and by a rigorous multipole method (GMM). The bulk optical constants of metals were modified by the size-limiting effect of nanoparticles. It was shown that a modified version of DDA [32] allows one to explain the shape of the experimental spectra for DLCA aggregates and the dependence of the spectra on the particle size.

3.3. Optical properties of clusters formed by biospecific aggregation. Correlation between the extinction spectra and cluster structure. In paper [22], we reported on the optical properties of aggregates formed by biospecific interactions like antigen/antibody, with one or both reaction components immobilized on gold particles. In the case of biospecific aggregation, the temporal changes in the absorption spectra differed from those recorded during rapid and slow salt aggregations. As in the case of rapid salt aggregation, the absorption peak decreased and shifted to the red part of the spectrum with simultaneous broadening. However, we did not observe the second red peak of the optical density. According to the transmission electron microscopy data, the slow, rapid, and biospecific aggregations resulted in small clusters with compact structures, branching aggregates of the fractal type, and aggregates without direct conductive contacts of the primary particles, respectively. It is supposed that the recorded differences in the absorption spectra can be explained by the corresponding differences in aggregate structures. We have found a direct correlation between the amount of the second added protein initiating aggregation on the one hand, and the rate of spectral changes on the other. Using these spectral changes, we have plotted a calibration curve for a sufficiently rapid and technically simple quantitative test like sol-particle immunoassay (SPIA).

Using TEM and spectrophotometry, we recorded three types of structures realized during the aggregation of colloidal-gold particles or bioconjugates, and also three types of the corresponding absorption-spectrum changes. In the slow salt aggregation, relatively small, compact aggregates form that have fractal dimension $d_f>2$. Such a type of aggregation is accompanied by small decreases in the main absorption-peak and by non-uniform widening of the long-wave wing. The rapid salt aggregation leads to the formation of fairly loose aggregates with the characteristic branching DLCA [22] structure and a fractal dimension of about 1.8. Contrary to the data of Ref. [42], we recorded in this case the presence of a second long-wave absorption peak for gold particles with direct ohmic contact. Finally, a characteristic of biospecific aggregates is

the presence of a biopolymer interlayer among the aggregate's gold particles, which prevents a direct conductive contact. The absorption-spectrum peak of such aggregates is reduced substantially and is shifted toward the red region, with the value of the peak decrease correlating with the concentration of the component initiating the aggregation of the conjugate.

3.4. A method for the differential spectroscopy of scattered light. Adsorption of a polymer onto the gold-particle surface results in relatively small changes in the optical density. The same is true for the initial stages of aggregation. Simple speculations [21] suggest that light scattering spectra can be more informative for adsorption of a polymer onto the particle surface, as well as for the initial stages of aggregation as compared to the absorption technique. Recently, we proposed a new method [43] to study biospecific interactions in systems of conjugates of colloidal gold nanoparticles. The method is based on measuring the differential spectra of light scattered at 90° within the wavelength range 350-800 nm. Addition of complementary components to the bioconjugate probe results in aggregation of nanoparticles that can be monitored by light scattering and extinction spectra. To this end, we have developed a special attachment to the Specord M-40 spectrophotometer and a corresponding measurement procedure called by us *differential light scattering spectroscopy*. The method has been compared with the usual spectrophotometry as applied to colloidal gold conjugated to various polymers including proteins and oligonucleotides. Our experiments with the gold particles of different sizes showed a higher potential sensitivity of the suggested method as compared with spectrophotometry. It is expected that the differential light scattering spectroscopy can be used to develop an analytical biospecific test for various biopolymers.

By contrast to known studies, in paper [43] we presented for the first time the experimental data about kinetic changes in extinction and scattering spectra caused by non-specific or biospecific aggregation of colloidal-gold conjugates. In both cases, already at 1-2 minutes after mixing the reagents we observed an essential increase in the resonance scattering maximum (up to 20 and even 400 times). Simultaneously, we recorded weaker changes in the extinction spectra. This observation allows one to assume that the developed light scattering technique can be used as a sensitive analytical test.

Fig. 8 shows an example of kinetic measurements of extinction and scattering spectra during biospecific aggregation. As a model system (designated as CG-15+PrA) conjugates of 15-nm particles to Protein A (Sigma, USA) were used. Aggregation was initiated by addition of the human IgG solution (Serva, Germany). The PrA molecule has two or more sites for biospecific binding of IgG molecules. Data in Fig. 8 correspond to an equimolar amount of reagent binding sites. Note how strongly the resonance scattering peak is increased in comparison with extinction spectral changes.

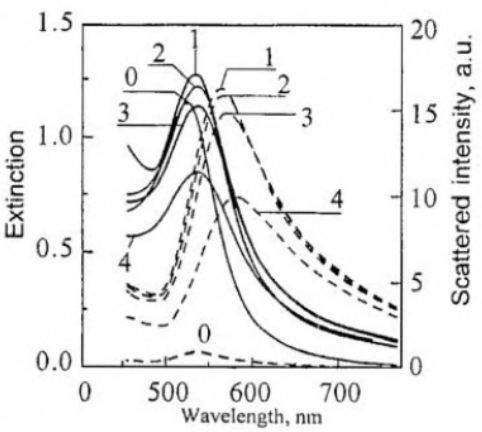

Fig. 8. Kinetics changes in extinction (solid lines) and right angle scattering (dashed lines) spectra of conjugates CG-15nm + Protein A (sample volume 4 ml; the gold number is 5 μg/ml). The numbers near curves correspond to the initial conjugate sol (0), and to the time intervals at 2 (1), 7 (2), 30 (3), and 90 (4) minutes after addition of 150 μl IgG at a concentration 1 mg/ml

3.5. Biological and medical applications of colloidal-gold markers. A pioneering biomedical application of colloidal gold was published by Maclagan in 1944 [44]. Since 1971, colloidal gold conjugates have been used traditionally in

immunocyto- and histochemical studies as markers for electron microscopy [45]. Gradually, the scope of use of gold markers was broadened. Currently, they are used in light microscopy methods and in various versions of force microscopy [46]. In addition, colloidal-gold conjugates are used in solid-phase-assay systems, such as dot-blot analysis [47], immunochroma-tographic test strips [48], and amplification of the immune response of experimental animals [49].

In our group, the fabricated colloidal-gold conjugates were used in studying the surface of nitrogen-fixing soil bacteria [24, 25] by TEM and dot-blot analysis [41] (perhaps, the first application of gold markers to dot-blot analysis of soil bacteria was described in 1989 [50]). Additionally, our markers and experimental procedures were used to develop an assay for a rapid diagnosis of acute enteric infections [26], as well as in studies of a proliferative antigen of the initial cells of a wheat stem meristem [27]. Recently, we recorded for the first time changes in the infrared spectra of Protein A-colloidal-gold conjugate after its interaction with immunoglobulin [51]. This result may serve as a basis for the development of new assay systems to detect biospecific interactions of the antigen-antibody type at *the single-molecule level.* Finally, one of the promising field, is the application of colloidal gold markers to preparation of antibodies both *in vitro* (by combinatorial phage display approach [28]), and *in vivo* (for amplification of the immune response [29]). Note that this intriguing amplification effect or, in other words, the adjuvant properties of gold sols have yet to be explained.

This work was partially supported by CRDF Grant № REC-006, and by RFBR Grants № 01-03-33130 and № 01-04-48736. We thank D.N. Tychinin (IBPPM RAS) for help in preparation of the manuscript, Yu-lin Xu (Univ. of Florida, USA) and Daniel Mackowski (Auburn Univ., USA) for the GMM computer codes.

References

1. *Schalkhammer Th.* Metal nano clusters as transducers for bioaffinity interactions // Chem. Monthly. 1998. V. 129. P. 1067.

2. *Lyon L.A., Musick M.D., Natan M.J.* Colloidal Au-enhanced surface plasmon resonance immunosensing // Anal. Chem. 1998. V. 70. P. 5177.

3. *Mulett W.M., Lai E.P.C., Yeung J.M.* Surface plasmon resonance-based immunoassays // Methods. 2000. V. 22. P. 77.

4. *Mirkin C.A., Letsinger R.L., Mucic R.C., Storhoff J.J.* DNA-based method for rationally assembling nanoparticles into macroscopic materials // Nature. 1996. V. 382. P. 607.

5. *Boal A.K., Ilhan F., DeRoucher J.E., Thurn-Albrecht Th., Rotello V.M.* Self-assembly of nanoparticles into structured spherical and network aggregates // Nature. 2000. V. 404. P. 746.

6. *Bohren C.F., Huffman D.R.* Absorption and Scattering of Light by Small Particles. -New York: Wiley, 1983.

7. *Khlebtsov N.G., Bogatyrev V.A., Dykman L.A., Melnikov A.G.* Optical properties of colloidal gold and its biospecific conjugates // Colloid J. 1995. V. 57. P. 384.

8. *Storhoff J.J., Lazarides A.A., Mucic R.C., Mirkin C.A., Letsinger R.L., Schatz G.C.* What controls the optical properties of DNA-linked gold nanoparticle assemblies? // J. Am. Chem. Soc. 2000. V. 122. P. 4640.

9. *Schatz G.S.* Electrodynamics of nonspherical nobel nanoparticles and nanoparticle aggregates // Theochem. 2001. V. 573. P. 73.

10. *Leuvering J.H., Thal P.J., van der Waart M., Schuurs A.H.* Sol particle immunoassay (SPIA) // J. Immunoassay. 1980. V. 1. P. 77.

11. *Ciesiolka T., Gabius H.-J.* An 8 to 10 fold enhancement in sensitivity for quantitation of proteins by modified application of colloidal gold // Anal. Biochem. 1988. V. 168. P. 280.

12. *Englebienne P., Van Hoonacker A., Valsamis J.* Rapid homogeneous immunoassay for human ferritin in the Cobas Mira using colloidal gold as the reporter reagent // Clin. Chem. 2000. V. 46. P. 2000.

13. *Englebienne P., Van Hoonacker A., Verhas M.* High-throughput using the surface plasmon resonance effect of colloidal gold nanoparticles // Analyst. 2001. V. 126. P. 1645.

14. *Khlebtsov N.G., Maksimova I.L., Tuchin V.V., Wang L.* Introduction to light scattering by biological objects // In: Handbook of Optical Biomedical Diagnostics / Tuchin V.V. (Ed.), -Bellingham, Washington: SPIE, 2002. P. 31.

15. *Khlebtsov N.G., Dykman L.A., Krasnov Ya.M., Melnikov A.G.* Extinction of light by aggregated gold particles and aggregated conjugates of gold particles to biospecific macromolecules // In: Electromagnetic and Light Scattering by Nonspherical Particles: Theory and Applications / Obelleiro F., Rodriguez J. L., Wriedt T. (Eds), -Vigo, Spain. 1999. P. 43.

16. *Khlebtsov N.G., Dykman L.A., Krasnov Ya.M., Melnikov A.G.* Light absorption by the clusters of colloidal gold and silver particles formed during slow and fast aggregation // Colloid J. 2000, V. 62. P. 765.

17. *Khlebtsov N.G.* An approximate method for calculating scattering and absorption of light by fractal aggregates // Opt. Spectrosc. 2000. V. 88. P. 594.

18. *Khlebtsov N.G.* Orientational averaging of the integral cross sections in the discrete dipole method // In: Light Scattering by Nonspherical Particles: Halifax Contributions / Videen G., Fu Q., Chylek P. (Eds), -Adelphy, Marylend: Army Research Laboratory, 2000. P. 123.

19. *Khlebtsov N.G., Dykman L.A., Bogatyrev V.A., Krasnov Ya.M., Medvedev B.A.* Extinction and scattering of light by gold nanoparticle clusters resulting from salt and biospecific aggregation // Ibid. P. 245.

20. *Khlebtsov N.G.* Orientational averaging of integrated cross sections in the discrete dipole method // Opt. Spectrosc. 2001. V. 90. P. 408.

21. *Bogatyrev V.A., Medvedev B.A., Dykman L.A., Khlebtsov N.G.* Light scattering spectra of colloidal gold aggregates: experimental measurements and theoretical simulations // In: Saratov Fall Meeting 2000: Optical Technologies in Biophysics and Medicine II / Tuchin V.V. (Ed.), Proc. SPIE, V. 4241. -Bellingham, Washington: SPIE, 2001. P. 42.

22. *Dykman L.A., Krasnov Ya.M., Bogatyrev V.A., Khlebtsov N.G.* Quantitative immunoassay method based on extinction spectra of colloidal gold bioconjugates // Ibid. P. 37.

23. *Bogatyrev V.A., Dykman L.A., Krasnov Ya.M., Plotnikov V.K., Khlebtsov N.G.* Biospecific assembling of gold nanoparticles with protein or oligonucleotide linkers as studied by light scattering and extinction spectra // In: Saratov Fall Meeting 2001: Optical Technologies in Biophysics and Medicine III / Tuchin V.V. (Ed.), Proc. SPIE, V. 4707. -Bellingham, Washington: SPIE, 2002 (in press).

24. *Egorenkova E.V., Konnova S.A., Fedonenko Yu.P., Dykman L.A., Ignatov V.V.* Role of the polysaccharide components of Azospirillum brasilense capsules in bacterial adsorption on wheat seedling roots // Microbiology. 2001. V. 70. P. 36.

25. *Chumakov M.I., Dykman L.A., Bogatyrev V.A., Kurbanova I.V.* Investigation of the cell surface structures of Agrobacteria involved in bacterial and plant interactions // Microbiology. 2001. V. 70. P. 232-238.

26. *Dykman L.A., Bogatyrev V.A.* Use of the dot-immunogold assay for the rapid

diagnosis of acute enteric infections // FEMS Immunol. Med. Microbiol. 2000. V. 27. P. 135-137.

27. *Sumaroka M.V., Dykman L.A., Bogatyrev V.A., Evseeva N.V., Zaitseva I.S., Shchyogolev S.Yu., Volodarsky A.D.* Use of the dot-blot immunogold assay to identify a proliferative antigen in the initial cells of a wheat stem meristem // J. Immunoassay. 2000. V. 21. P. 401-410.

28. *Sumaroka M.V., Dykman L.A., Bogatyrev V.A., Zaitseva I.S., Sokolov O.I., Shchyogolev S.Yu., Harris W.J.* Preparation, selection and immunodetection of antibodies to low-molecular-weight compounds by using hapten-colloidal gold conjugates and combinatorial phage libraries // Allergology and immunology. 2000. V. 1. P. 134-135.

29. *Dykman L.A., Sumaroka M.V., Staroverov S.A., Zaitseva I.S., Bogatyrev V.A.* The immunogenicity of colloidal gold // Biol. Bull. 2002 (in press).

30. *Khlebtsov N.G., Melnikov A.G.* Structural anisotropy of fractal clusters and orientational optic effects in transmitted light // Colloid J. 1998. V. 60. P. 781.

31. *Draine B.T.* Electromagnetic scattering by compounded spherical particles // In: Light scattering by Nonspherical Particles / Mishchenko M.I., Hovenier J.W., Travis L.D. (Eds), San Diego: Academic Press, 2000. P. 131.

32. *Markel V.A., Shalaev V.M., Stechel E.B., Kim W., Armstrong R.L.* Small-particle composites. I. Linear optical properties // Phys. Rev. B. 1996. V. 53. P. 2425.

33. *Yu-lin Xu.* Electromagnetic scattering by an aggregate of spheres. // Appl. Opt.1995. V. 34. P. 4573.

34. *Fuller K.A., Mackowski D.W.* Electromagnetic scattering by compounded spherical particles // In: Light Scattering by Nonspherical Particles: Theory, Measurements, and Applications / Mishchenko M.I., Hovenier J.W., Travis L.D. (Eds), - San Diego: Academic Press, 2000. P. 225.

35. *Khlebtsov N.G.* Orientational averaging of light scattering observables in the T-matrix approach // Appl. Opt. 1992. V. 31. P. 5359.

36. *Khlebtsov N.G., Bogatyrev V.A., Dykman L.A., Melnikov A.G.* Spectral extinction of colloidal gold and its biospecific conjugates // J. Colloid Interface Sci. 1996. V. 180. P. 436.

37. *Lazarides A.A., Schatz G.C.* DNA-linked metal nanosphere materials: Structural basis for the optical properties // J. Phys. Chem. B. 2000. V. 104. P. 460.

38. *Lazarides A.A., Schatz G.C.* DNA-linked metal nanosphere materials: Fourier-transform solutions for the optical response // J. Chem. Phys. 2000. V. 112. P. 2967.

39. *Nath N., Chilkoti A.* A colorimetric gold nanoparticle sensor to interrogate biomolecular interactions in real time on a surface // Anal. Chem. 2002. V. 74. P. 504.

40. *Eck D., Helm Ch.A., Wagner N.J., Vaynberg K.A.* Plasmon resonance measurements of the absorption and adsorption kinetics of a biopolymer onto gold nanocolloids // Langmuir. 2001. V. 17. P.957.

41. *Dykman L.A., Bogatyrev V.A.* Colloidal gold in solid-phase analysis. A review // Biochemistry (Moscow). 1997. V. 62. P. 350.

42. *Danilova Yu.E.* Localization of Optical Excitations in Colloidal Silver Aggregates. PhD Thesis, Inst. Automatics and Electrometry RAS, Novosibirsk, 1999.

43. *Bogatyrev V.A., Dykman L.A., Krasnov Ya.M., Plotnikov V.K., Khlebtsov N.G.* A method of differential spectroscopy of scattered light for studies of biospecific assembling of gold nanoparticles with protein or oligonucleotide probes // Colloid J. 2002 V. 64. № 6.

44. *Maclagan N.F.* The serum colloidal gold reaction as a liver function test // Brit. J. Exp. Pathol. 1944. V. 25. P. 15.

45. *Faulk W., Taylor G.* An immunocolloid method for the electron microscope // Immunochemistry. 1971. V. 8. P. 1081.

46. *Neagu C., van der Werf K.O., Putman C.A.J., Kraan YM., de Grooth B.G., van Hulst N.F., Greve J.* Analysis of immunolabeled cells by atomic force microscopy, optical microscopy, flow cytometry // J. Struct. Biol. 1994. V. 112. P. 32.

47. *Moeremans M., Daneels G., van Dijck A., Langanger G., De Mey J.* Sensitive visualization of antigen-antibody reactions in dot and blot immune overlay assays with immunogold and immunogold/silver staining // J. Immunol. Methods. 1984. V. 74. P. 353.

48. *Shyu R.H., Shyu H.F., Liu H.W., Tang S.S.* Colloidal gold-based immunochromatographic assay for detection of ricin // Toxicon. 2002. V. 40. P. 255.

49. *Shiosaka S., Kiyama H., Wanaka A., Tohyama M.* A new method for producing a specific and high titre antibody against glutamate using colloidal gold as a carrier // Brain Research. 1986. V. 382. P. 399-403.

50. *Bogatyrev V.A., Ivanova L.Yu., Schwartsburd B.I., Khlebtsov N.G.* Use of colloidal gold in immunodot technique // 19th Meeting FEBS, Rome, July 2-7, 1989. Abstr. Book, P. 30.

51. *Kamnev A.A., Dykman L.A., Tarantilis P.A., Polissiou M.G.* Surface-enhanced Fourier transform infrared spectroscopy of protein A conjugated with colloidal gold // In: Metal Ions in Biology and Medicine, V. 7 / Khassanova L., Collery Ph., Maymard I., Khassanova Z., Etienne J.-C. (Eds), -Paris: John Libbey Eurotext, 2002. P. 104.

Institute of Biochemistry and Physiology of Plants and Microorganisms
Saratov State University

Received 21.05.2002

УДК 535.36

ОПТИЧЕСКИЕ СВОЙСТВА БИОКОНЪЮГАТОВ КОЛЛОИДНОГО ЗОЛОТА

Н.Г. Хлебцов, В.А. Богатырев, Л.А. Дыкман, Я.М. Краснов, А.Г. Мельников

Обсуждаются оптические свойства единичных и агрегированных конъюгатов коллоидного золота, которые синтезируются при адсорбции биополимеров на поверхности золотых наночастиц. Для моделирования ослабления и рассеяния света подобными структурами использована обобщенная теория Ми для произвольной мультисферной конфигурации рассеивателей и метод дискретных диполей вместе с компьютерной моделью кластер-кластерной агрегации. В первой части статьи обсуждаются следующие вопросы: • статистическое и ориентационное усреднение оптических наблюдаемых параметров; • оптические эффекты, связанные с линейными цепочками наночастиц; • влияние полимерного покрытия и межчастичного расстояния на оптические свойства агрегатов; • моделирование кинетических изменений оптических свойств агрегированных золей, формируемых в процессе биоспецифического связывания конъюгатов; • модификация мультипольного подхода для случая двухслойных мономеров. Во второй части статьи дается краткий обзор наших экспериментальных исследований по синтезу, теоретическому моделиро-ванию и практическому применению биомаркеров на основе коллоидного золота (включая биомедицинские приложения), и приводятся экспериментальные примеры оптического мониторинга биоспецифических взаимодействий на нанометровом масштабе.

Khlebtsov Nikolai Grigor'evich (1949, Astrakhan), Head of Biophysics Group at the Institute of Biochemistry and Physiology of Plants and Microorganisms, Russian Academy of Sciences, Saratov, Russia; also Professor at the Department of Optics, Saratov State University. Graduated from the Saratov State University in 1972. Doctor of Physical and Mathematical Sciences (1996), PhD (1982). Field of research: Optics of Disperse Systems, Fractal Clusters, Electro-optical Effects in Suspensions and High Polymer Solutions, Radiative Transfer and Light Scattering, Remote Sensing of Atmosphere and Ocean, Biophysics of Microbial Populations. He has about 120 scientific publications.

E-mail: khlebtsov@ibppm.saratov.su

Bogatyrev Vladimir Alexandrovich (1958, Monchegorsk), Senior researcher of Biophysics Group at the Institute of Biochemistry and Physiology of Plants and Microorganisms, Russian Academy of Sciences. Graduated from the Saratov State University in 1980, PhD (candidate of biological sciences, 1995). Field of research: Electro-optical effects in microbial suspensions, synthesis and application of colloidal-gold biomarkers. He has about 90 scientific publications.

Dykman Lev Abramovich (1962, Saratov), Head of Immunotechnology Group at the Institute of Biochemistry and Physiology of Plants and Microorganisms, Russian Academy of Sciences. Graduated from the Saratov Medical Institute in 1985. PhD of Biology (1996). Field of research: immunology; immunochemistry; microbiology; colloidal chemistry and optics of gold sols. He has about 70 scientific publications.

Krasnov Yaroslav Mikhailovich (1971, Kamyshin), Graduate student of Biophysics Group at the Institute of Biochemistry and Physiology of Plants and Microorganisms. Graduated from the Saratov State University in 1985. Field of research: Synthesis and biomedical application of colloidal-gold conjugates, experimental studies of optical properties of aggregated gold nanoparticles. He has 10 scientific publications.

Melnikov Andrei Gennadievich (1963, Saratov), Senior researcher of Biophysics Group at the Institute of Biochemistry and Physiology of Plants and Microorganisms. Graduated from the Saratov State University in 1985, PhD from Saratov State University (candidate of physic and mathematical sciences, 1982). Field of research: computer simulation of light absorption and scattering by small particles and aggregates. He has about 40 scientific publications.